DINAME 2023 - Proceedings of the XIX International Symposium on Dynamic Problems of Mechanics,
A.S. De Paula, A.T. Fabro and M.R. Machado (Editors), ABCM.
Pirenópolis, Go, Brazil, February 26th to March 3rd, 2023

Challenges in rotor dynamics: from identification of uncertain parameters to balancing techniques

Katrin Ellermann[1], **Marcel S. Prem**[1], **Georg Quinz**[1], **and Michael Klanner**[1]

[1] Institute of Mechanics, Graz University of Technology, Kopernikusgasse 24, 8010 Graz, Austria

Abstract: This paper presents computational techniques for the analysis of rotating machinery. The modeling of the dynamic behavior of these machines needs to account for various effects, some of which are related to parameters with a significant amount of uncertainty. The work can be divided into three main parts: The first part describes the numerical assembly technique (NAT). NAT is a modelling technique that provides (semi-)analytical solutions for the equations of motion of slender structures, such as a shaft of an electrical machine.
The second part then applies this model in combination with measured frequency response functions in order to find suitable values for material parameters. The third part uses the model and appropriate material parameters to balance the rotor. The proposed balancing technique uses the measured response of the rotor but does not need trail weights for the balancing procedure.

Keywords: parameter identification, balancing, numerical assembly technique, rotor dynamics

INTRODUCTION

From a mechanical point of view, modelling a machine with rotating parts holds various challenges: Considering an electrical machine, the various components like shaft, rotor stack, copper windings, resin, all have very different material properties. The contacts between these components not only contribute to the overall damping of the machine but also may change during operation due to nonlinear geometric effects and temperature changes. In addition, vibrations are influenced by external loads or time-delay effects resulting from the rotation.

Simulation techniques can assist in getting a better understanding of the machine during the design process. They can also be useful for the safe operation. This paper addresses different techniques to model rotating machines efficiently and to reduce the uncertainty in the system. These techniques allow for new approaches to balance the rotor and operate the machine.

In the following, we use a special modelling procedure in order to identify the material properties of a shaft of a rotor.

NUMERICAL ASSEMBLY TECHNIQUE (NAT)

There are various techniques to model the vibrations of machines and machine components. By now, numerical techniques are probably the most common, especially techniques involving the Finite Element Method (FEM). FEM is versatile and can be used for structures of very different sizes and shapes. Many FEM tools are highly developed and numerically optimized so it is relatively easy to use them, even if there may be simpler methods that could reach the same accuracy of prediction.

In general, numerical techniques are computationally expensive and hide the effect of specific parameters on the overall response. This might be acceptable if the equations are evaluated only once and if all parameters are known precisely. When parameters are not known precisely, and repetitive evaluations of the equations are needed, more efficient models are of great value.

For components with a relatively simple geometry – like the shaft of a rotor, the dynamics can be described very precisely even without numerical techniques. There are different analytical approaches modelling slender components based on beam theories.

For a shaft of a rotor, the length is significantly greater than the dimensions of the cross-section. Analytical approaches based on the Euler-Bernoulli or the Timoshenko beam theories are therefore often a better choice: Beam theories exhibit only a very small error due to simplifying modelling assumptions, such as the assumption that cross-sections of the beam remain plane and perpendicular to the axis of the beam, or the neglect of deformation due to shear (in case of the Euler-Bernoulli theory). For slender components, the error due to these modelling assumptions can usually be neglected. On the other hand, these approaches allow for an analytical solution for the dynamics of the beam.

Here, the shaft of the rotor is modeled by the so-called Numerical Assembly Technique (NAT). Figure 1 shows a section of the shaft. This section is characterized by its length ℓ_i, diameter d_i, and material parameters considered in Young's modulus E. Masses $m^{(i)}$ and mass moments of inertia $\Theta^{(i)}$ are accounted for at the stations, which are located at the ends of a section. The section may have external loads, such as point forces F_p, point moments M_p or distributed

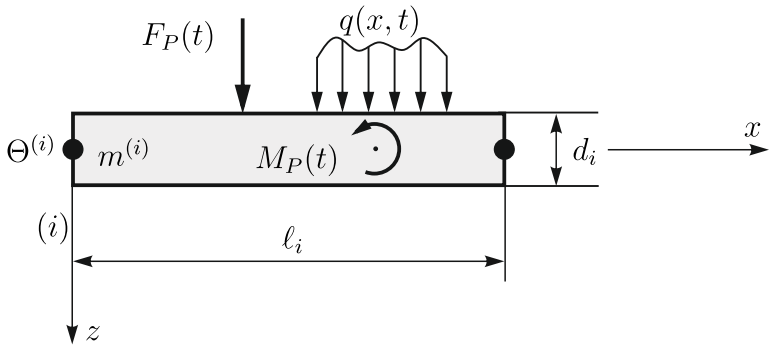

Figure 1 – Numerical assembly technique: model of a section

loads q. For simplicity, only distributed loads are considered in the following.

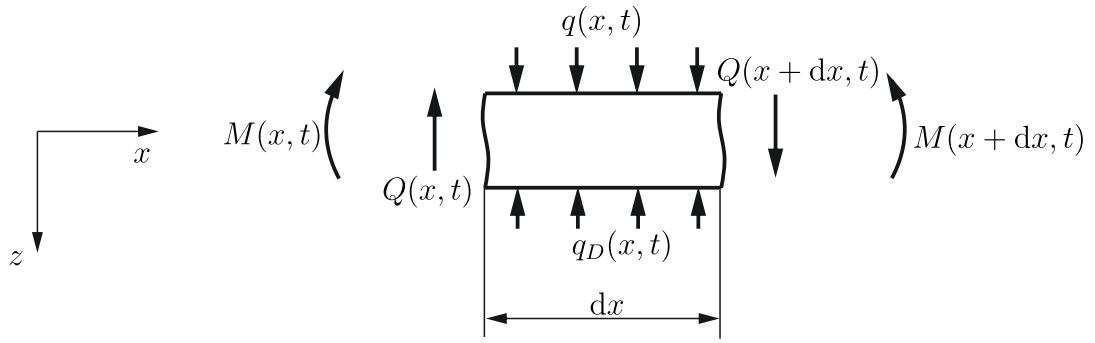

Figure 2 – Infinitesimal part of a Timoshenko beam

Given the infinitesimal part of a Timoshenko beam shown in Figure 2 with the internal shear force $Q(x,t)$, the internal bending moment $M(x,t)$ and the distributed forces due to external loads $q(x,t)$ and external viscous damping $q_D(x,t)$, then Newton's law is given by

$$\rho A \frac{\partial^2 w(x,t)}{\partial t^2} - \frac{\partial Q(x,t)}{\partial x} - q(x,t) + q_D(x,t) = 0, \tag{1}$$

and similarly Euler's law results in

$$\rho I \frac{\partial^2 \varphi(x,t)}{\partial t^2} - \frac{\partial M(x,t)}{\partial x} + Q(x,t) = 0. \tag{2}$$

Herein, ρ is the density of the material, A is the cross-section of the beam, I is the second moment of the area of the cross-section. For the external viscous damping a damping law

$$q_D(x,t) = d_a \frac{\partial w(x,t)}{\partial t} \tag{3}$$

is assumed.

The deflection of the beam and the rotation of the cross-section are given by w and φ. According to the Timoshenko beam theory, the total deflection w is composed of two parts: a component w_b due to bending and a component w_s due to shear. The bending is the reason for the rotation of the cross-section, leading to

$$\varphi(x,t) = \frac{\partial w_b(x,t)}{\partial x}. \tag{4}$$

By integration over the cross-sectional area, the stresses are linked to the internal loads. This leads to

$$M(x,t) = \int\int_A \sigma_{xx}(x,z,t)\, z \,\mathrm{d}A \tag{5}$$

$$Q(x,t) = \int\int_A \sigma_{xz}(x,t)\,\mathrm{d}A \tag{6}$$

with the normal stress σ_{xx} and the shear stress σ_{xz}.

On the other hand, given a suitable material law, the stresses are also linked to the deformation of the beam. In the simplest case, the material is described by a linear stress-strain relation (Hooke's law). However, not all materials are suitably described by a linear relation. Given that machines with slender shafts are prone to vibrations, all sources of damping are especially important for the dynamics.

Material laws based on fractional calculus have become increasingly important for viscoelastic materials. These material laws include a time-dependency between stress and strain so that changes in strain result in high stresses, whereas a constant strain over some time leads to decreasing stress. This effect also gives a damping effect in the overall structure.

Mathematically, this time-dependency can be described by

$$\sigma(t) = c_\beta \frac{\mathrm{d}^{\beta_{\text{Power}}}\varepsilon(t)}{\mathrm{d}t^\beta}, \tag{7}$$

where c_β is assumed to be a constant coefficient. The so-called fractional derivative of the strain $\varepsilon(t)$ has two special cases, which are simple to interpret in a mechanical sense: for $\beta_{\text{Power}} = 0$, the equation (7) describes a linear spring, for $\beta_{\text{Power}} = 1$ it corresponds to a linear damper. Allowing for values $0 < \beta_{\text{Power}} < 1$ gives more generalized material models. Taking this idea even further leads to material models which also include time derivatives of the strain to give

$$\sigma(t) + \sum_{i=1}^{n_\varepsilon} b_i \frac{\mathrm{d}^i\sigma(t)}{\mathrm{d}t^i} = a_0\varepsilon(t) + \sum_{i=1}^{m_\sigma} a_i \frac{\mathrm{d}^i\varepsilon(t)}{\mathrm{d}t^i}, \tag{8}$$

where a_0, a_i and b_i are constant values.

For the stresses in (5) and (6), we use a material law given by

$$\sigma_{xx}(x,z,t) + b_0^E \frac{\partial^{\alpha^E}\sigma_{xx}(x,z,t)}{\partial t^{\alpha^E}} = a_0^E \varepsilon_{xx}(x,z,t) + a_1^E \frac{\partial^{\alpha^E}\varepsilon_{xx}(x,z,t)}{\partial t^{\alpha^E}}, \tag{9}$$

$$\sigma_{xz}(x,t) + b_0^G \frac{\partial^{\alpha^G}\sigma_{xz}(x,t)}{\partial t^{\alpha^G}} = a_0^G \gamma_{xz}(x,t) + a_1^G \frac{\partial^{\alpha^G}\gamma_{xz}(x,t)}{\partial t^{\alpha^G}}. \tag{10}$$

The shear strain is denoted by γ. The other symbols α^*, a_*^* and b_*^* stand for positive real constants, which are yet unknown quantities.

Using a Fourier transformation, this leads to a stress-strain relation of the form

$$\tilde{\sigma}_{xx}(x,z,\omega) = \frac{a_0^E + (\mathrm{j}\omega)^{\alpha^E} a_1^E}{1 + b_0^E (\mathrm{j}\omega)^{\alpha^E}} = \mathrm{E}^\star(\omega)\tilde{\varepsilon}_{xx}(x,z,\omega), \tag{11}$$

$$\tilde{\sigma}_{xz}(x,\omega) = \frac{a_0^G + (\mathrm{j}\omega)^{\alpha^G} a_1^G}{1 + b_0^G (\mathrm{j}\omega)^{\alpha^G}} = \mathrm{G}^\star(\omega)\tilde{\gamma}_{xz}(x,\omega), \tag{12}$$

where $\mathrm{E}^\star(\omega)$ and $\mathrm{G}^\star(\omega)$ are the frequency-dependent complex Young's modulus and the frequency-dependent complex shear modulus.

The equations (1) and (2) are then solved for steady-state vibration with frequency ω. In this step, the dependencies on time and space are decoupled by enforcing that for each quantity $\star = \star(x,t)$ there is a complex amplitude $\tilde{\star}(x)$ such that

$$\star(x,t) = \tilde{\star}(x)\,\mathrm{e}^{\mathrm{j}\omega t}. \tag{13}$$

This results in (see Klanner et al., 2021)

$$\begin{aligned} &\frac{\mathrm{d}^4 w(x)}{\mathrm{d}x^4} + \left(\bar{\omega}^2(1+\bar{E}) - \bar{d}_a(\omega)\right)\frac{\mathrm{d}^2 w(x)}{\mathrm{d}x^2} + \bar{\omega}^2\left(\bar{\omega}^2\bar{E} - \frac{1}{r_G^2} - \left(1 - \frac{1}{\bar{E}\,r_G^2\,\bar{\omega}^2}\right)\bar{d}_a(\omega)\right) w(x) = \\ &\frac{1}{\kappa_S GA}\left(\left(\frac{1}{\bar{E}\,r_G^2} - \bar{\omega}^2\right) q(x) - \frac{\mathrm{d}^2 q(x)}{\mathrm{d}x^2}\right), \end{aligned} \tag{14}$$

$$\varphi(x) = \frac{-\bar{E}\,r_G^2}{1 - \omega^2\,\bar{E}\,r_G^2}\left(\frac{\mathrm{d}^3 w(x)}{\mathrm{d}x^3} + \left(\frac{1 + \omega^2\,\bar{E}^2\,r_G^2}{\bar{E}\,r_G^2} - d_a(\omega)\right)\frac{\mathrm{d}w(x)}{\mathrm{d}x} + \frac{1}{\kappa_S GA}\left(\frac{\mathrm{d}q(x)}{\mathrm{d}x}\right)\right), \tag{15}$$

$$M(x) = E\,I\,\frac{\mathrm{d}\varphi(x)}{\mathrm{d}x}, \tag{16}$$

$$Q(x) = \kappa_S\,G\,A\left(\varphi(x) + \frac{\mathrm{d}w(x)}{\mathrm{d}x}\right), \tag{17}$$

with the shear correction factor κ_S, the shear modulus G and the coefficients

$$\bar{\omega}^2 = \frac{\rho\,\omega^2}{E}, \quad \bar{E} = \frac{E}{\kappa_S\,G}, \quad r_G^2 = \frac{I}{A}, \quad d_a(\omega) = \frac{\mathrm{j}\,d_a\,\omega}{\kappa_S\,G\,A}.$$

Solving the governing equation leads to two components. One is given by the homogeneous solution – representing the free vibration. The other constitutes a particular solution – which considers the forcing terms. These solutions may be expressed in analytical form – unless the loading requires a numerical formulation.

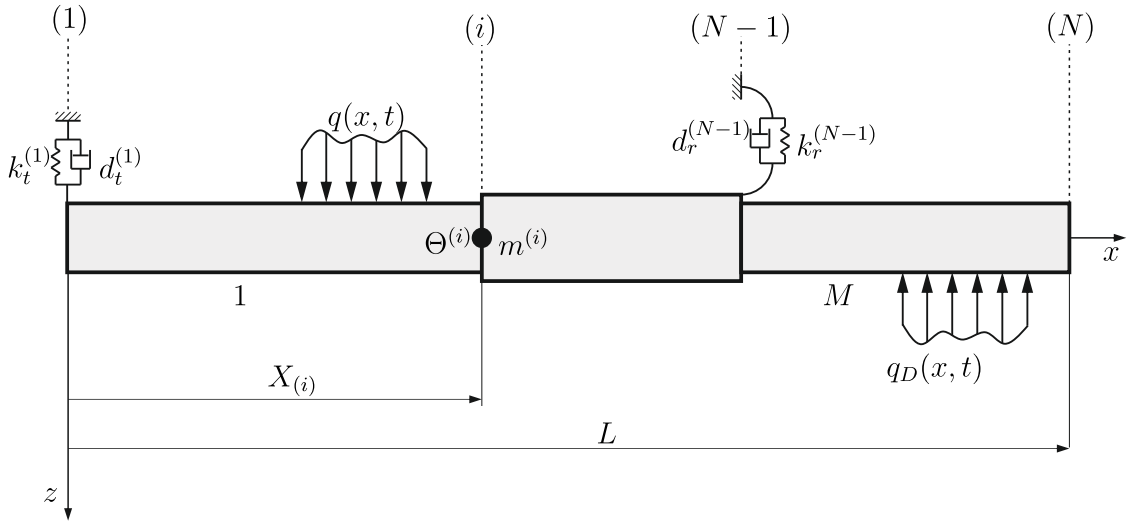

Figure 3 – Numerical assembly technique: combining sections to a complete model of a shaft

In practice, the description of the shaft of a rotor requires more than just one smooth beam as formulated before. Changes along the shaft, such as different cross-sections or localized loads due to supports (bearings) or rotor discs, require that the shaft is divided into different sections as symbolically shown in Figure 3. The individual sections are characterized by analytical equations as derived above. The different sections are then combined by enforcing the boundary and interface conditions. For more details on the NAT-model, see Klanner et al. 2021.

The NAT-model of the shaft has various parameters. Some of these parameters are directly given from the design of the machine or are relatively easy to measure, like the length ℓ_i of a section or its diameter d_i. Here, the material parameters are considered more critical. In a fractional derivative description of the so-called Zener model, the complex Young's modulus is described by four parameters: a_0, a_1, b_0 and the exponent α.

$$\mathrm{E}(\mathrm{j}\omega) = \frac{a_0 + a_1(\mathrm{j}\omega)^\alpha}{1 + b_1(\mathrm{j}\omega)^\alpha}, \tag{18}$$

Determining the parameters a_0, a_1, b_0 and α from an experimental frequency response curve for a given shaft is the aim of the parameter estimation.

PARAMETER ESTIMATION

In order to evaluate the model for a simulation of the dynamical behavior, numerical values for all parameters are needed. Here, the procedure focuses on parameters which contribute a significant amount of uncertainty to the system. Geometric properties are assumed to be known precisely.

Given the NAT-model and the fractional Zener model described in the previous section, the material parameters a_0, a_1, b_1 and the exponent α are to be determined from frequency response functions (FRF). The following parameter estimation follows the idea also presented by Prem et al., 2021.

The process is based on experimental data from a frequency response test. Figure 4 shows the schematic test setup. The shaft is suspended by fishing lines, which are attached to the ends of the shaft. This type of support essentially

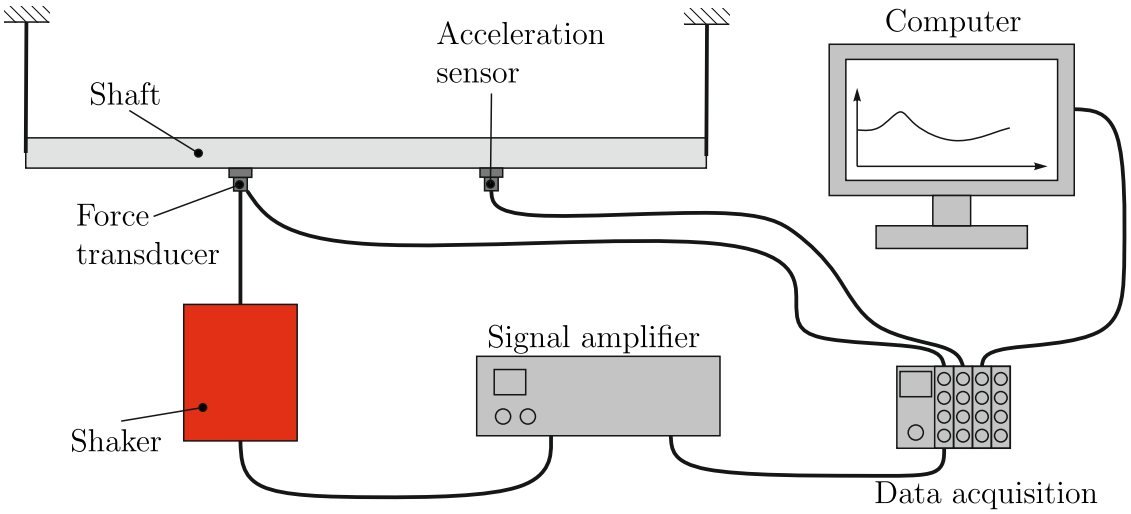

Figure 4 – Schematically representation of the test setup for the parameter estimation

corresponds to a free-free boundary condition. Then, the shaft is excited harmonically by a shaker at one point, and the response is measured using an acceleration sensor attached at a specific position of the shaft. Depending on the positions of the excitation and the measured response, an FRF curve is obtained.

The characteristic shape of the FRF curve depends on several parameters of the experimental setup, including the material of the shaft. Figure 5 shows an example of such a curve. In this case, the curve shows three distinct eigenfrequencies (EF) within the range investigated. The amplitudes of the peaks at these eigenfrequencies are marked by AMP.

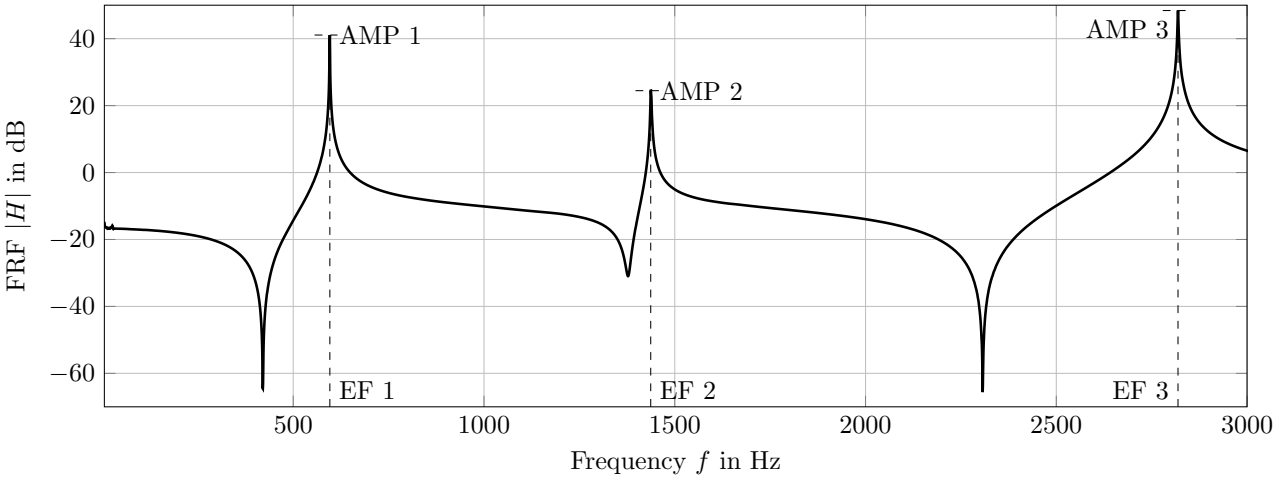

Figure 5 – Example of an FRF curve

For the subsequent determination of the material parameters, the eigenfrequencies, the amplitudes at the eigenfrequencies (both as shown in Figure 5) and the so-called quality factor Q are used as reference values. The quality factor is defined as a dimensionless quantity describing the width of the peak at an eigenfrequency as given by

$$Q = \frac{\mathrm{EF}}{\Delta f}, \tag{19}$$

where the width Δf of the peak is evaluated $3dB$ below AMP. This procedure is commonly known as half-power method. Therefore, for a measured FRF curve with n distinct eigenfrequencies, there are $3n$ reference values that are to be matched by the corresponding values obtained from a simulated response. Assuming numerical values for all model parameters,

these reference values are determined from the NAT-model. Comparing the simulated values with the experimental ones then shows, if the assumed parameter values were suitable for the simulation or not.

Different strategies can be applied to find suitable parameter values. Here, the process starts without any information on the parameters, so a wide range of numerical values is considered. This wide range is then first reduced by a bisectioning process: The reference values are computed for the maximum values of the parameter range, the minimum values and one in the middle. The value in the middle then shows if the upper half or the lower half contains suitable values. This process is repeated several times until the parameter range is smaller than a prescribed limit value or the middle value does not clearly show whether the upper or lower half of the interval contains the suitable values.

After this coarse refinement of the interval, a more refined analysis is performed, which looks for an optimum within the remaining interval. In principle, this can be done by a Monte-Carlo analysis. However, even though the numerical model is relatively efficient, there is still a significant numerical effort when thousands of combinations of different parameter values are evaluated. Therefore, substitute models are used in order to reduce the numerical effort.

Here, the substitute model is based on a polynomial chaos expansion (PCE), see e. g. Marelli et al. The procedure involves two steps: In the first step, the reference values of each eigenfrequency are considered separately to find a surrogate model for this specific eigenfrequency. This first step is needed to limit the allowed parameter range to only those values which give a good match for all eigenfrequencies. Parameter values that provide a good fit for only some eigenfrequencies, but are way off for others, are eliminated. In the second step, a new surrogate model is determined, allowing for a global minimization of the reference values of all eigenfrequencies.

As the first test of this parameter identification, the procedure was used on a numerically generated test case: When using an FRF curve generated numerically from a known set of parameter values, the procedure should be capable of identifying these parameter values precisely. For this test case, the results converged quickly to the exact values.

Afterwards, the procedure was applied to shafts from our test stand. The shafts are all very similar in size but made of different materials: steel, aluminium and different synthetic and compound materials.

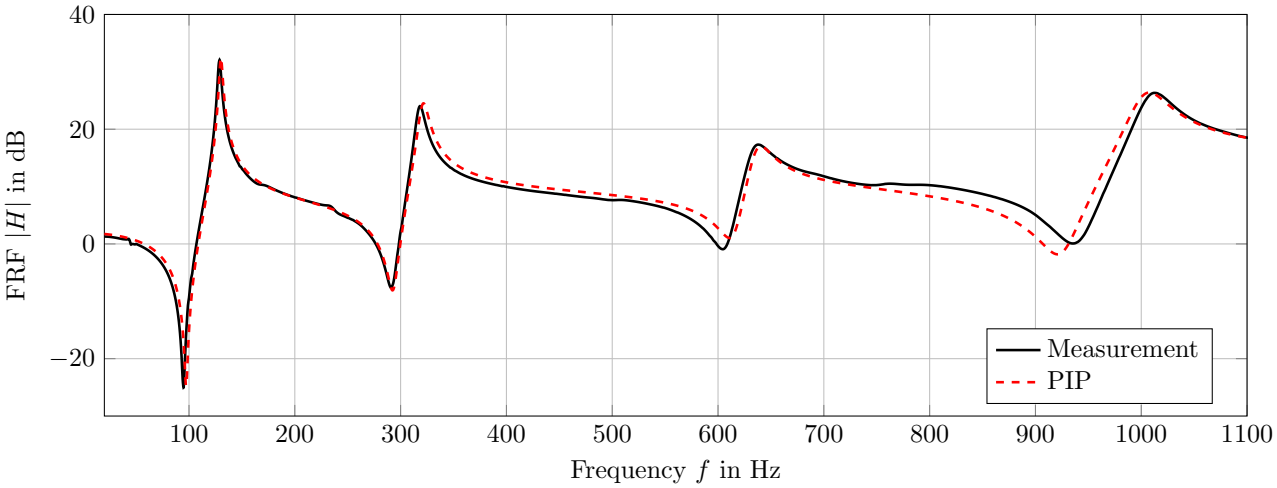

Figure 6 – Reference FRF curve and estimated FRF curve - Synthetic material

As an example, Figure 6 shows the results for a synthetic material (polyethylene). This material shows relatively high damping compared to metal shafts, especially at high frequencies. The parameters identified from the described process give a very close match for low frequencies. For high frequencies, the estimated eigenfrequencies and amplitude values are still determined within a few percent of the measured ones, but in between, the curve deviates from the measured curve even if the trend is still followed well.

For material that has a low damping, the process gives even better results. The process was also tested for compound material, which is non-isotropic and has a non-homogeneous structure. As almost expected, for these material properties, the results gave a general trend of the curve, but the match between the measured and estimated response was not satisfactory. More refined material models are currently under investigation.

BALANCING

Given the efficient way to model a shaft with one or more disks and the material parameters obtained in the parameter estimation process, this information is then used to balance the rotor of a machine. An imperfect mass distribution causes the unbalance of a shaft or an entire rotor including the rotor discs. Balancing the rotor aims to counteract the imperfection

of the mass distribution of the rotor by adding small balance weights. Figure 7 shows the rotor setup used for balancing in this study.

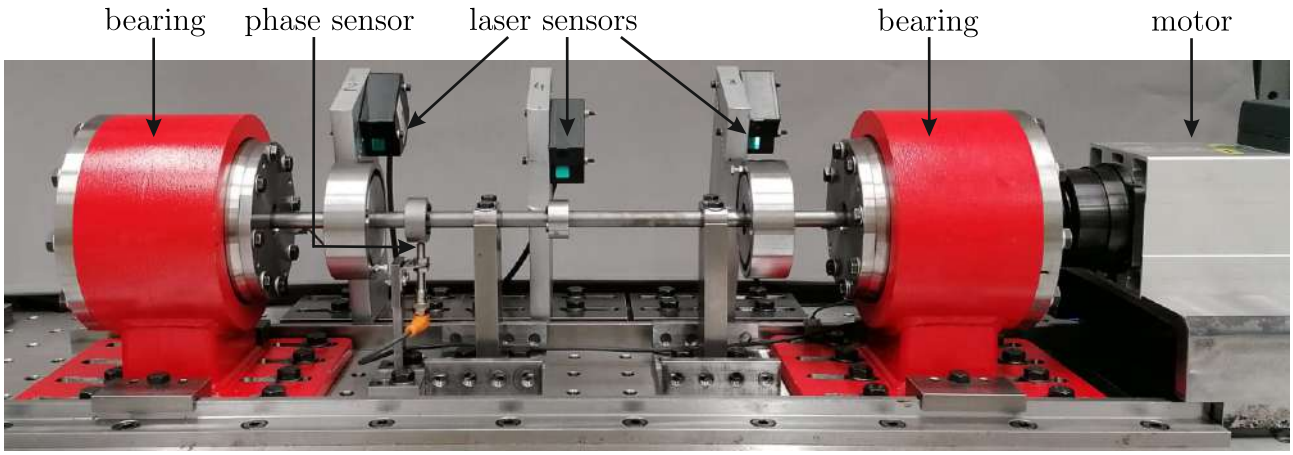

Figure 7 – Experimental setup for balancing procedure

Good combinations of position and mass of the balance weights can be found in different ways. Several techniques are based on the concept of influence coefficients, see also Thearle, 1934: These coefficients measure the ratio between added unbalance and the resulting change in the vibration response. Initially, the influence coefficient method was applied for rigid rotors, where two balancing planes are sufficient for balancing. The concept was later extended to include the flexibility of the shaft and multiple balancing planes.

The influence coefficients are defined as

$$\alpha_{ik}(\Omega) = \frac{w_i(\Omega)}{U_k}. \tag{20}$$

Herein, $w_i\Omega$ is the displacement at position i caused by the unbalance U_k at position k. Measuring these influence coefficients is very time-consuming as it requires various measurements with different unbalance weights at different positions. In our case, the coefficients are calculated from the NAT model. Then combining all the different numerical results from different (assumed) unbalance masses yields the influence coefficient matrix $\underline{\underline{\alpha}}$

$$\vec{w} = \underline{\underline{\alpha}}\vec{U}, \tag{21}$$

where $\vec{w}$ combines the displacements caused by adding test weights in the numerical calculation. The vector $\vec{U}$ combines the different unbalance weights. This approach is therefore based on the assumption of linearity so that the effects of different test masses add up to a total response (superposition).

Solving (21) for $\vec{U}$ for a given vector of displacements $\vec{w}$ then gives the distribution of the unbalance

$$\vec{U} = \underline{\underline{\alpha}}^{-1}\vec{w}. \tag{22}$$

Evaluating this for the measured response $\vec{w}_0$, which has no test masses but only the initial unbalance of the rotor, then allows for the determination of the required correction $\vec{U}_c$ as

$$\vec{U}_c = -\underline{\underline{\alpha}}^{-1}\vec{w}_0. \tag{23}$$

The vibrational response depends on the unbalance and the spin speed. This also affects the influence coefficients, and thus the computed balance weights. Least-square approaches are therefore used to minimize the unbalance at different positions and for different spin speeds.

Balancing using influence coefficients requires four steps:

- Selection of balancing planes and relevant spin speeds: Balance masses are added to (or removed from) the rotor at specific locations, the so-called balance planes that are parallel to the xy-plane.

- The vibrational response of the (unbalanced) rotor is measured for every balance plane and spin speed.
- The changes in the vibrational response caused by test weights added in each balance plane are determined.
- Influence coefficients and balance weights are calculated.

Most conventional techniques require a significant number of trial runs with test masses in order to determine the influence coefficients and the resulting balance weights. This is costly and time consuming. In order to reduce this effort, several approaches were presented which replace the experimental test-runs by computational techniques. The effect of additional masses at the rotor on the dynamic response is thus determined numerically, in most cases by finite element models, see e. g. Bin et al., 2013.

Here, we use the information from the NAT-model to compute influence coefficients. This procedure reduces the effort for balancing significantly, see also Quinz et al., 2021.

Balancing always includes experimental data of the rotor that is to be balanced. In this case, the rotor displacement is measured by laser sensors and the angular position during the rotation by an inductive phase sensor, see Figure 7.

A set of measurements considers the rotor's initial (unbalanced) state, where the vibrations are determined near the critical speeds. In these measurements close to the eigenfrequencies, the effect of the unbalance is most obvious – measurements far away from the eigenfrequencies would give only small amplitudes, and the change due to the unbalance is hidden within other effects like a small amount of measurement noise. On the other hand, it is obviously not safe to operate an unbalanced rotor at an eigenfrequency for a prolonged amount of time in order to get a good estimation of the steady state response. Therefore, the estimation of the steady-state response is obtained within a frequency range that exhibits response amplitudes within an allowable range and then the experiment is stopped when the permissable amplitude is reached.

For the experimental setup shown in Figure 7, the first two eigenfrequencies are at 59.107 Hz and 145.483 Hz. Figure 8 shows the response of the rotor without any balance weights.

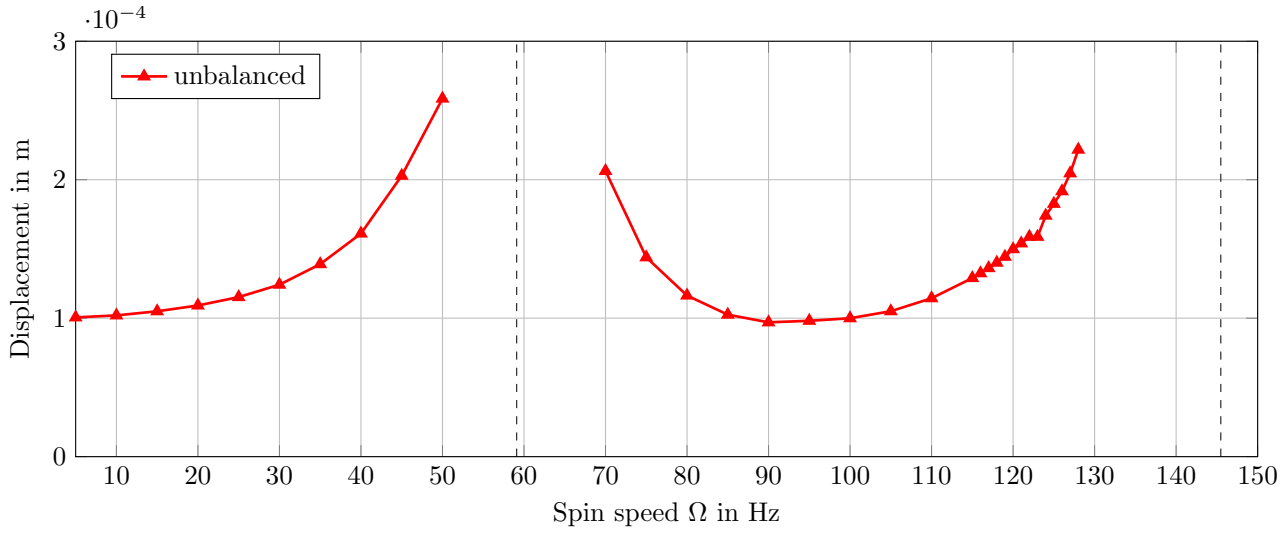

Figure 8 – Response of the unbalanced rotor

The numerical assembly technique, again, is used to model the shaft as schematically shown in Figure 9. The model is similar to the one used in the parameter identification process. In addition to describing the different sections of the shaft, the model here accounts for the support due to the bearings (shown as springs and dampers) and the additional masses due to the rotor discs and the clutch. The red markers $\vec{U}$ symbolically show unbalance weights (test weights) of the rotor. The exact position of this unbalance is yet unknown.

In order to find the required balancing weights, the numerical model of the rotor is evaluated near the critical speeds for various magnitudes and positions of the unbalance masses. This procedure could be considered as numerical replacements for experimental test with trial weights. The numerical calculations give information on eigenfrequencies, mode shapes and unbalance responses.

The approach considers a modal composition of the balancing procedure. The modal matrix derived from the NAT-model allows for balancing each mode separately. The positions for each mode's balance weights are determined such that other modes are not influenced.

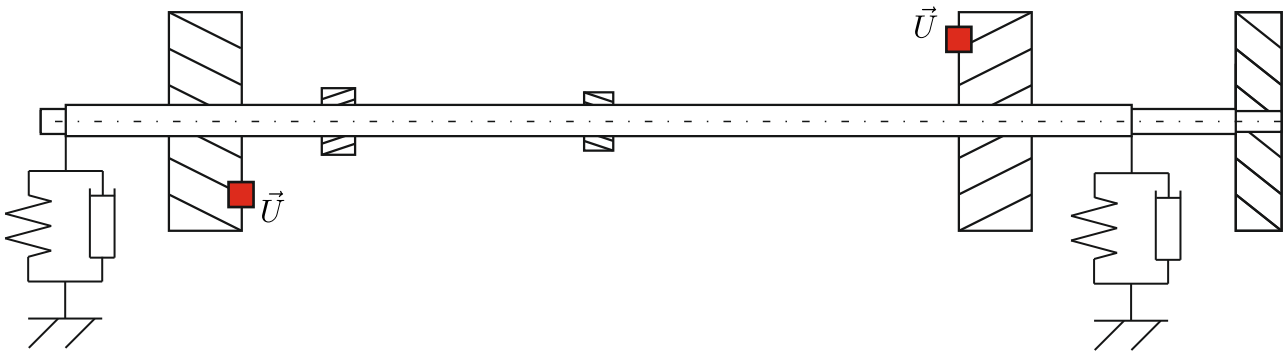

Figure 9 – Schematics of the numerical model

In order to balance N different modes, the corresponding shapes of these N bending modes need to be known. The rotor's vibrations need to be measured at N or more positions along the shaft, and also N different planes need to be considered for the positions of the balancing weights. For precise balancing, the vicinity of nodes of eigenmodes needs to be excluded.

The described procedure is then applied to balance this rotor and thus reduce the vibration amplitudes near the two eigenfrequencies. The measurements are evaluated at 50 Hz and 119 Hz. The calculation of the required balance weights takes approximately 0.03 s using the NAT model. Thus, using the digital model of the rotor instead of experimental test runs makes the balancing procedure significantly faster.

Figure 10 shows the result of the balancing procedure compared to the initial response. Evaluating the amplitudes at 50 Hz, that is near the first eigenfrequency, gives a reduction of 85 % at the left and of 77 % at the right rotor disc. Similarly, the amplitudes evaluated near the second eigenfrequency were found to reduce the vibrations at 128 Hz, by 77 % at the left and by 21 % at the right disk.

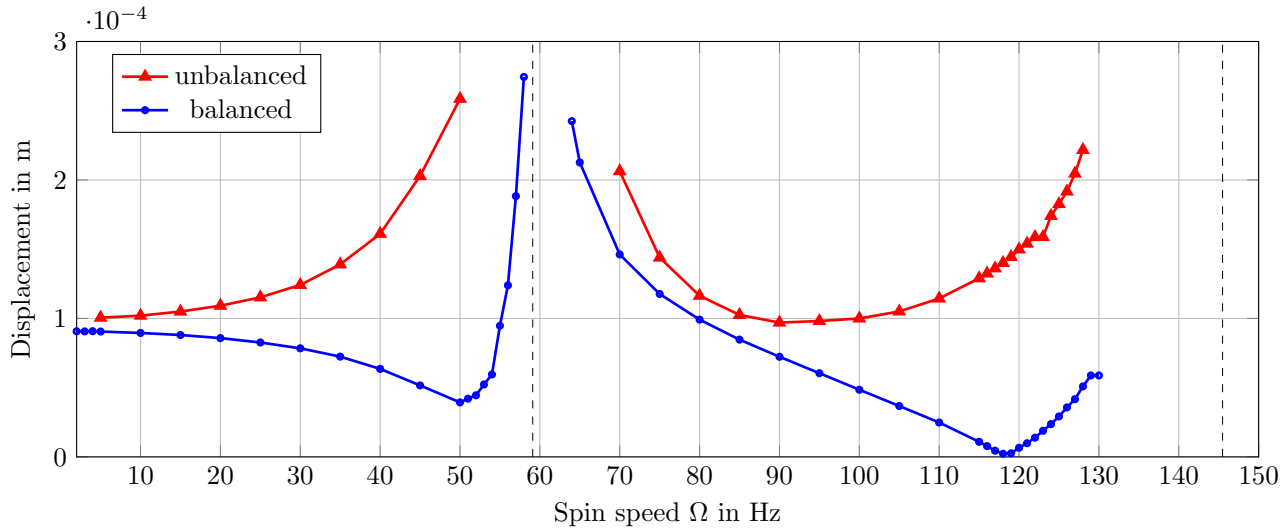

Figure 10 – Balancing result

CONCLUSION

The numerical assembly technique (NAT) was found to be an efficient modelling technique capable of describing the vibrations of slender structures. Such vibrating slender structures are commonly found in rotor dynamics.

This paper describes how the NAT is first applied to find the material properties of the shaft of a rotor – whereby special attention is given to properties that lead to material damping. The parameter values of a fractional Zener model were found to provide a good description of most shafts made of homogeneous isotropic material.

These material properties then form the basis of further steps, such as a balancing procedure. Rotor discs were

assembled on the shaft, and the shaft was then mounted in a test stand. Using just one measurement, giving the frequency response of the unbalanced setup and the influence coefficients calculated from a numerical procedure, the rotor was balanced, and the amplitudes of the vibrations near the eigenfrequencies were significantly reduced.

Further investigations will include more refined material descriptions, allowing for non-isotropic and non-homogenous properties of the structure.

REFERENCES

Klanner, M., Prem, M. S. and Ellermann, K., 2021, "Steady-State Harmonic Vibrations of Viscoelastic Timoshenko Beams with Fractional Derivative Damping Models", Applied Mechanics, Vol. 2 (4), https://www.mdpi.com/2673-3161/2/4/46.

Prem, M. S., Klanner, M. and Ellermann, K., 2021, "Identification of Fractional Damping Parameters in Structural Dynamics Using Polynomial Chaos Expansion", Applied Mechanics, Vol. 2 (4), https://www.mdpi.com/2673-3161/2/4/56.

Marelli, S.,Lüthen, N., Sudret, B., 2021 "UQLab user manual – Polynomial chaos expansions, Tech. rep., Chair of Risk, Safety and Uncertainty Quantification", ETH Zurich, Switzerland, report UQLab-V1.4-104.

Thearle, E.L., 1934 "Dynamic Balancing of Rotating Machinery in the Field", Trans. ASME, 56, pp. 745-753.

Bin, G., Yao, J., Jiang, Z., Gao, J., 2013, "Solving method of influence coefficient for rotor dynamic balance based on finite element model", J. Vib. Meas. Diagn. 33 908-1002.

Quinz, G., Prem, M. S., Klanner, M. and Ellermann, K., 2021, "Balancing of a linear elastic rotor-bearing system with arbitrarily distributed unbalance using the Numerical Assembly Technique", Bulletin of the Polish Academy of Sciences: Technical Sciences, Vol. 69 (6), http://journals.pan.pl/Content/120482/PDF/SS6_08_02270_Bpast.No.69(6)_OK.pdf.

RESPONSIBILITY NOTICE

The authors are the only responsible for the printed material included in this paper.